Journal of Alloys and Compounds 795 (2019) 19–26

Contents lists available at ScienceDirect

Journal of Alloys and Compounds

journal homepage: http://www.elsevier.com/locate/jalcom

Grain growth and Hall-Petch relationship in a refractory HfNbTaZrTi high-entropy alloy

Shuying Chen [a], Ko-Kai Tseng [b], Yang Tong [a], Weidong Li [a, **], Che-Wei Tsai [b, c], Jien-Wei Yeh [b, c], Peter K. Liaw [a, *]

[a] Department of Materials Science and Engineering, The University of Tennessee, Knoxville, TN 37996, USA
[b] Department of Materials Science and Engineering, National Tsing Hua University, Hsinchu, 30013, Taiwan
[c] High Entropy Materials Center, National Tsing Hua University, Hsinchu, 30013, Taiwan

ARTICLE INFO

Article history:
Received 14 January 2019
Received in revised form
24 April 2019
Accepted 26 April 2019
Available online 7 May 2019

Keywords:
Grain growth
Hall-Petch relation
Mechanical properties

ABSTRACT

Understanding the effect of temperature variation on the microstructural evolution is particularly important to refractory high-entropy alloys (RHEAs), given their potential high-temperature applications. Here, we experimentally investigated the grain-growth behavior of the HfNbTaZrTi RHEAs during recrystallization at temperatures from 1,000 to 1,200 °C for varied durations, following cold rolling with a 70% thickness reduction. Following the classical grain-growth kinetics analysis, two activation energies are obtained: 205 kJ/mol between 1,000 and 1,100 °C, and 401 kJ/mol between 1,100 and 1,200 °C, which suggests two mechanisms of grain growth. Moreover, the yield strength − grain size relation was found to be well described by the Hall-Petch relation in the form of $\sigma_y = 942 + 270D^{-0.5}$. It was revealed that the friction stress, 942 MPa, in the HfNbTaZrTi HEA is higher than that of tungsten alloys, which indicates the high intrinsic stress in the BCC-RHEA. The coefficient, 270 MPa/μm $^{-1/2}$, is much lower than that in the 316 stainless steel and $Al_{0.3}$CoCrFeNi HEAs, which indicates low grain-boundary strengthening.

1. Introduction

High-entropy alloys (HEAs) were coined by Yeh [1] in 2000's, and have attracted the rapidly-increasing attention in the past decade due to their stabilized microstructures and remarkable mechanical properties [2,3]. HEAs typically consist of five or more metallic elements in equal or nearly-equal atomic percent and are inclined to form solid solution phases including body-center-cubic (BCC) [3–5], face-center-cubic (FCC) [6–9], and hexagonal-close-packed (HCP) structure [10–13] by the stabilization of the high configurational entropy [7,14]. Prior research has demonstrated that HEAs possess superior properties in many facets, including high yield strength [14], good microstructural stability, retained mechanical strength at elevated temperatures [15,16], and excellent resistance to wear [17], corrosion [18,19], creep [20,21], fracture [22], and fatigue [23–30].

Studying the grain-growth behavior of HEAs is important, as the improper thermal exposure may significantly degrade an alloy's mechanical properties, e.g., fatigue-strength drop. But sluggish diffusion, considered as one of the core effects for HEAs, can stabilize grains by slowing down their growth. Liu et al. [31] investigated the grain growth of the CoCrFeMnNi HEAs in a temperature range of 850 °C–950 °C and determined the activation energy for growth to be 321.7 kJ/mol. Wu et al. [32] reported a grain-growth exponent of 4 in the CoCrFeNi HEA at 900 °C. Sathiaraj et al. [33] found that the sluggish diffusion in the CoCrFeMnNi HEAs can significantly influence the texture development during the grain growth. However, it remains unclear whether this phenomenon is general to RHEAs.

Painting a clear picture about the grain growth and its effect on mechanical properties in RHEAs is even more important than doing so in non-refractory HEAs, simply because RHEAs are primarily targeted for high-temperature applications and are expected to expose to elevated temperatures for long durations. The HfNbTaZrTi RHEA is becoming of great interest recently because it manifests excellent softening resistance at elevated temperatures, making it very promising for high-temperature applications [15]. Also, this BCC HfNbTaZrTi RHEA has outstanding phase stability at temperatures greater than 1,000 °C [15] and excellent malleability

* Corresponding author.
** Corresponding author.
E-mail addresses: wli20@utk.edu (W. Li), pliaw@utk.edu (P.K. Liaw).

https://doi.org/10.1016/j.jallcom.2019.04.291
0925-8388/

at low temperatures. Senkov et al. [34] first conducted a preliminary investigation on the grain growth in this RHEA upon cold rolling and annealing. Juan et al. [35] performed a detailed study on the cold-rolled (70% thickness reduction) as-cast HfNbTaZrTi RHEA in a temperature range of 1,200–1,350 °C, and reported the grain-growth exponent and activation energy to be 3.5 and 389 kJ/mol, respectively. The later work by Senkov et al. [36] examined the grain-growth kinetics in a homogenized, cold-forged, and then cold-rolled (89% thickness reduction) HfNbTaZrTi RHEA at 800–1,200 °C, and suggested a grain-growth exponent of 2 and activation energy of 246 kJ/mol. However, opposite conclusions can be drawn based on the considerably different values from these two studies. The major difference between these two cases is the sample processing. In an as-cast HfNbTaZrTi RHEA, compositional heterogeneity exists in dendrite and inter-dendrite regions [34], which can impose a significant influence on the grain growth due to the solute-dragging effect. On the other hand, the cold-forging treatment [36] can highly induce the dynamic recovery and dynamic recrystallization, which should not be ignored when comparing these two studies.

To reduce the extrinsic effects mentioned above, the present work examined the grain-growth behavior during annealing in the lower temperature range, 1,000, 1,100 and 1,200 °C, on the cold-rolled as-cast HfNbTaZrTi RHEA. The intent is to offer a complementary viewpoint on the grain-growth kinetics in the HfNbTaZrTi RHEA. Meanwhile, the effect of grain size on its mechanical properties was also studied.

2. Material and experimental procedures

The HfNbTaTiZr RHEA ingots were prepared by arc melting the constituent elements [purity > 99.9 weight percent (wt.%)] in a water-cooled copper crucible under the argon atmosphere. To ensure the compositional homogeneity, the melts were overturned and re-melted for multiple times prior to dropping to copper molds for solidification. After finishing the round slugs from the bowl-shape copper mold, several slugs were re-melted again in the rectangular mold with the cavity dimensions 20 × 30 × 60 mm. The slab ingots were machined into the dimensions of 13.5 × 25 × 50 mm for the subsequent cold-rolling process. There is no homogenization treatment prior to rolling. Individual reduction per pass was 0.2 mm. Specimens were cold-rolled to a final thickness of 4 mm (a thickness reduction of 70%). The cold-rolled sheets were then sealed in vacuum-quartz tubes and annealed at 1,000, 1,100, and 1,200 °C for 0.5, 2, 6, and 24 h, followed by water quenching. All heat-treated samples were ground and polished on a Buehler rotating grinder and polisher to remove surface defects, with the 400, 600, 800, and 1,200 grit sandpapers used in sequence. Then samples were placed on the vibratory polisher for 24 h, with polishing suspension of colloidal silica of 0.05 μm to obtain the final polished specimens with mirror surface. No etching was performed. The average grain sizes of differently-processed alloys were determined by applying the linear intercept method to microscopic images taken from the scanning electron microscope (SEM, Zeiss, EVO MA15).

The possible phases in differently-treated alloys were identified through X-ray diffraction (XRD, Panalytical Empyrean) with the Cu Kα radiation. The detailed parameters are: slit: soller slits 0.04 rad; mask: fixed incident beam mask 10 mm; step size: 0.013; speed: 0.05/s, respectively. The detailed microstructures in these alloys were examined with the SEM equipped with back-scattered diffraction. The acceleration voltage and filament current are 20 kV and 1 nA, respectively. The flat dog-bone-shaped tensile specimens are machined to have the gauge length of 19 mm, thickness of 1 mm, and gauge section width of 3 mm. Tensile tests were carried out on selected RHEA samples with different grain sizes at room temperature and a strain rate of 1×10^{-4}/s.

3. Results

3.1. Phase and microstructure

After undergoing the cold-rolling reduction with a 70% thickness reduction and annealing at 1,000, 1,100, and 1,200 °C for 0.5, 2, 6, and 24 h, the HfNbTaZrTi HEAs exhibits a single BCC phase. Some representative XRD patterns samples annealed at 1,000–1,200 °C for 0.5 h are shown in Fig. 1. No second phases except a single BCC phase form at this temperature range.

During the annealing treatment, the elongated grains originated from cold rolling are consumed and turned into equiaxed grains after experiencing nucleation and growth stages. The recrystallized grains of the samples after being annealed at 1,000–1,200 °C for 0.5 and 24 h were characterized with backscattered-electron (BSE) imaging, as given in Fig. 2. One microstructural feature worth emphasizing is that the equiaxed grains attained in the alloys are not uniform in size for all annealing conditions, as evidenced by the mixture of coarse and fine grains on the images of microstructures. Size variation in the recrystallized grains may be related with the varied energy storage in grains during the cold-rolling process, which is the driving force of recrystallization and grain growth [34].

3.2. Grain-growth kinetics

Grain growth of the HfNbTaZrTi RHEA upon annealing was further quantitatively analyzed in this section. We first plot the average grain size as a function of the annealing temperature at the annealing time of 0.5–24 h in Fig. 3. The grain size increases with the increase of both the annealing temperature and time. For a given annealing time, the variation of the grain size with the temperature approximately follows a linear trend. The rate of grain growth is slow at 1,000 °C, but gradually becomes faster when the temperature ramps up to 1,100 and 1,200 °C. The average grain sizes measured for the HfNbTaZrTi HEAs under various annealing conditions in the present work are listed in Table 1. Alongside we also compile from the literature the grain sizes of the same HEA that

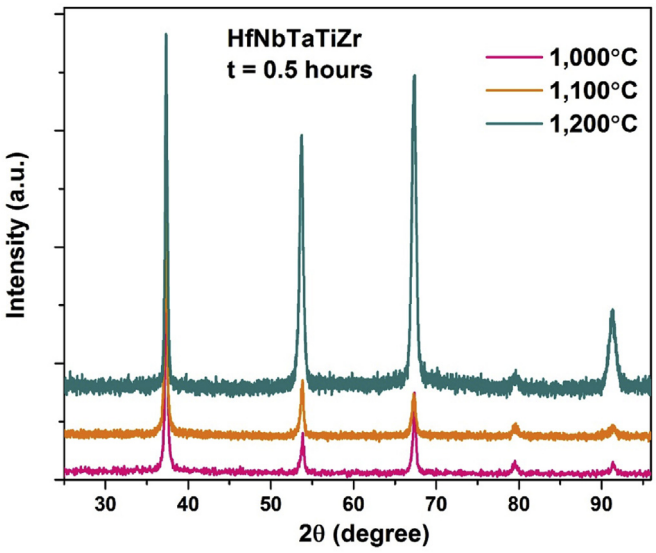

Fig. 1. XRD patterns of the HfNbTaTiZr HEAs annealed at 1,000, 1,100, and 1,200 °C for 0.5 h.

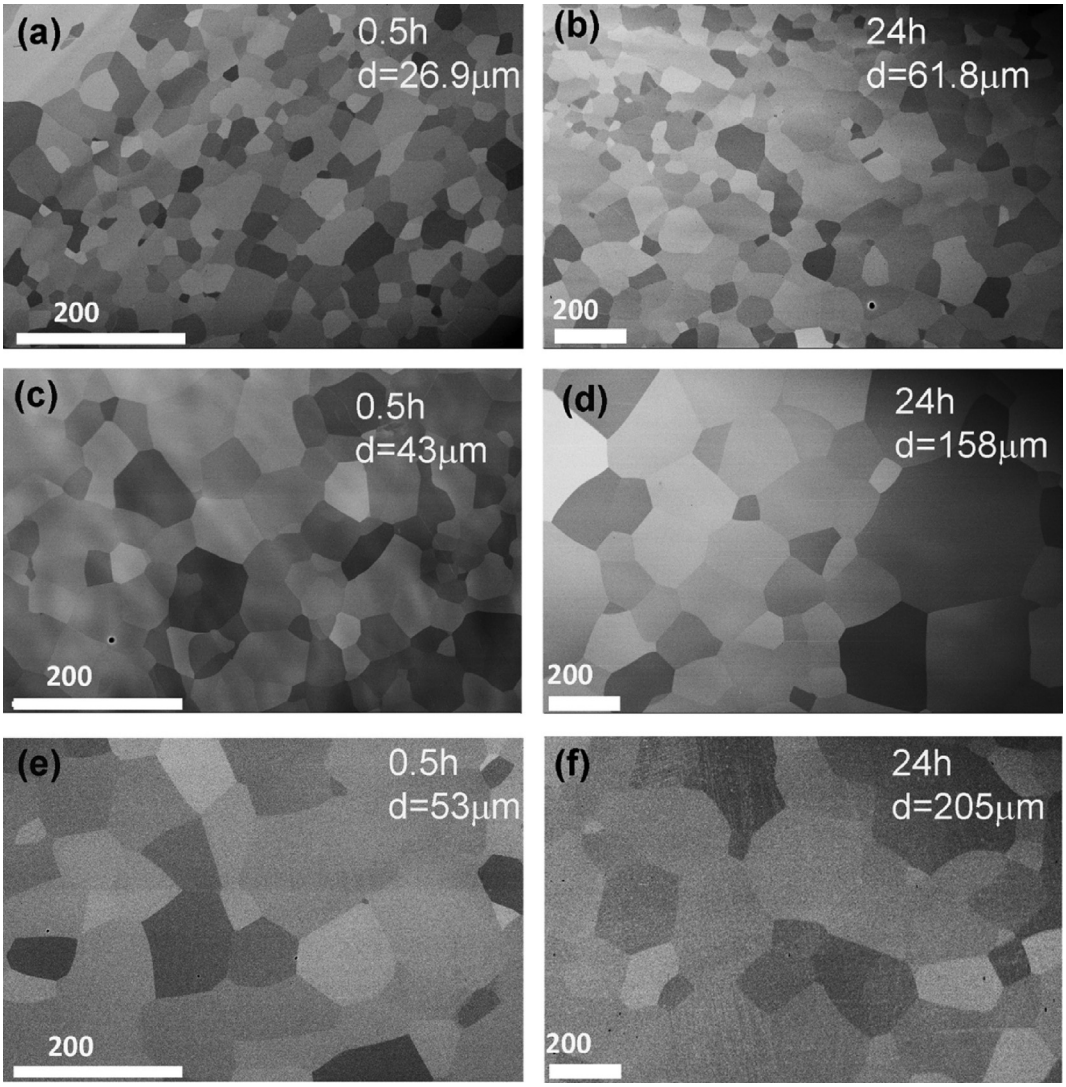

Fig. 2. SEM images of the microstructures of the HEAs, annealed at 1,000 °C for (a) 0.5 and (b) 24 h, 1,100 °C for (c) 0.5 and (d) 24 h, and 1,200 °C for (e) 0.5 and (f) 24 h.

have experienced similar heat treatments [34,36]. Comparing the results in Table 1, we found that the grain size drops, as the thickness reduction increases during cold rolling. For instance, when annealed at 1,000 °C for 2 h, the average grain sizes are 35, 31.5, 22, and 21.9 μm for the alloy with a thickness reduction of 65% [34], 70%, 84.6% [34], and 89% [36], respectively. The declining trend of the grain size with increasing the thickness reduction during cold rolling is most likely associated with the variation in the available grain-nucleation sites in differently-deformed alloys. In heavily-deformed materials, a fairly-large amount of defects, including dislocation structures, grain boundaries, and other deformation heterogeneities, such as deformation bands [33], are potential sites for new grains to nucleate. As a consequence, compared to the counterparts with less deformation, more grains participate in competition among the course of recrystallization, resulting in a slower grain growth rate [33,37].

The grain-growth kinetics in metals can be quantified by a parabolic model proposed by Burke and Turnbull [38]. The model was constructed, based on the hypothesis that recrystallized grains grow by grain-boundary migration. For the sake of the minimization of the grain-boundary area and the associated energy, the rate of the boundary migration is thought of being inversely proportional to the radius of the curvature of grain boundaries, further to the diameter of grains [39]. Eventually, the evolution of the grain size over time is expressed as [40,41].

$$D^n - D_0^n = kt \tag{1}$$

where t is the time, D_0 is the initial grain size (at $t = 0$), D is the grain size at the time, t, for a given temperature, n is the grain-growth exponent, and k is a constant depending on the material composition and temperature. In the work previously reported, D_0 is crudely treated as zero by assuming $D \gg D_0$ [31,35]. This approximate treatment will undoubtedly cause errors when determining the value of n, and later the activation energy, posing questions on the credibility of the conclusions derived thereafter. To avoid any uncertainty caused by approximation, here we use a differential method to treat D_0 explicitly. Specifically, we first take differentiation to both sides of Eq. (1) with respect to t, getting

$$\frac{dD^n}{dt} - \frac{dD_0^n}{dt} = k \cdot \frac{dt}{dt} \tag{2}$$

Since D_0 is a constant, we have $\frac{dD_0^n}{dt} = 0$, Eq. (2) reduces to

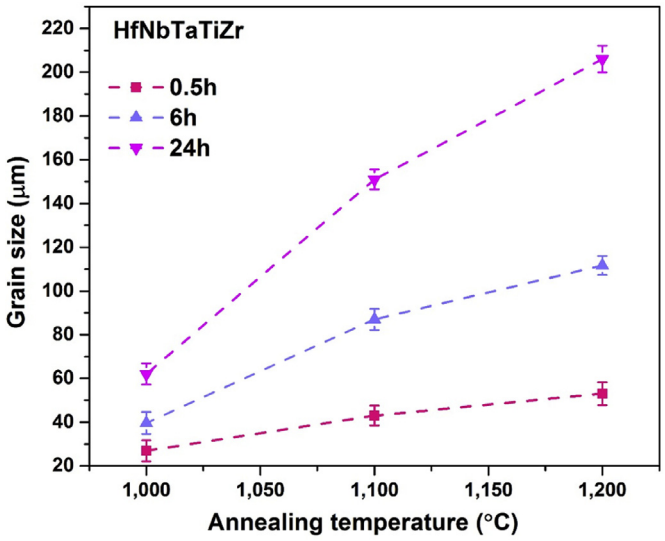

Fig. 3. The variations of the average grain sizes of the HfNbTaTiZr HEAs with the annealing temperature and time. The average grain sizes are determined by applying the linear-intercept method to the SEM images of the microstructures.

Table 1
The average grain sizes of the HfNbTaTiZr HEAs, including our samples cold-rolled to a 70% thickness reduction and annealed at various temperatures and times, as well as those compiled from literature [34,36].

Temperature (°C)	*t* (h)	D (μm) 70%	D (μm) [34]		D (μm) [36] 89%
			65%	84.6%	
1,000	0.5	27	–	–	–
	2	31.5	35	22	21.9
	6	39.1	–	–	–
	24	62	–	–	–
1,100	0.5	43	–	–	24.4
	2	62.5	–	–	38.4
	6	87	–	–	–
	24	151	–	–	–
1,200	0.5	53	–	–	–
	2	79	91	76	75.5
	6	111.7	–	–	–
	24	206	–	–	–

$$\frac{dD^n}{dt} = k \tag{3}$$

Given that D is a function of time t, i.e., $D = f(t)$, Eq. (3) can be further written as

$$\frac{dD^n}{dD}\cdot\frac{dD}{dt} = k \tag{4}$$

and then

$$n\cdot D^{(n-1)}\cdot\frac{dD}{dt} = k \tag{5}$$

Taking the natural logarithm (or common logarithm) to both sides of Eq. (5), we have the following

$$\ln\left(n\cdot D^{(n-1)}\cdot\frac{dD}{dt}\right) = \ln k \tag{6}$$

$$\ln n + \ln D^{(n-1)} + \ln\frac{dD}{dt} = \ln k \tag{7}$$

$$\ln n + (n-1)\ln D + \ln\frac{dD}{dt} = \ln k \tag{8}$$

Rearranging Eq. (8), we arrive

$$\ln\frac{dD}{dt} = -(n-1)\ln D + \ln k - \ln n \tag{9}$$

$$\ln\frac{dD}{dt} = -(n-1)\ln D + \ln\frac{k}{n} \tag{10}$$

Now we can use Eq. (10) to fit the experimental data.

The slope of the fitting curve is -(n-1), the intercept is $\ln\frac{k}{n}$. Knowing n and $\ln\frac{k}{n}$, k is determined from

$$k = n\cdot e^{intercept} \tag{11}$$

The grain-growth data at different temperatures is plotted in the form of ln(dD/dt) against ln$D$ and linearly fitted in Fig. 4. From the slopes and intercepts of the linear fits, the n and k values for the HfNbTaZrTi HEAs annealed at 1,000, 1,100, and 1,200 °C are determined and listed in Table 2. It is noted that the n values, 2.2–2.4, in the present work are close to the n values, 2 or 3 (prefer 2), obtained at 1,100 °C by Senkov et al. [36] in a homogenized, cold-forged, and then cold-rolled HfNbTaZrTi RHEA. But when compare the n value, 3.5, obtained at 1,200–1350 °C by Juan et al. [35], there seems a discrepancy at 1,200 °C. The reason for this might be due to different annealing times used: 0.5, 6 and 24 h in the present work and 10, 30, 60, 360 min in the report of [35]. Longer annealing time tends to give smaller exponent n since the specimen thickness

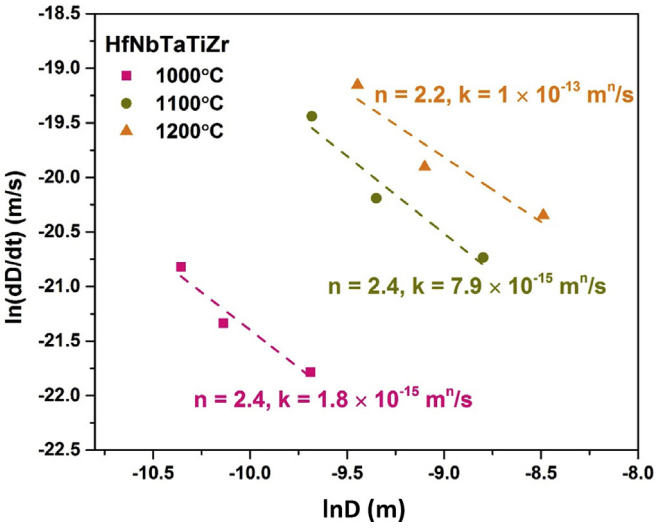

Fig. 4. Linear fitting of Eq. (10) to the logarithm of the average grain size versus the logarithm of the dD/dt for the HfNbTaTiZr HEAs annealed at 1,000, 1,100, and 1,200 °C. From the slopes, the values of the grain growth-exponents, n, are determined.

Table 2
The n and k values evaluated at different annealing temperatures.

Temperature (°C)	n	k (m^n/s)
1,000	2.4	1.8×10^{-15}
1,100	2.4	7.9×10^{-15}
1,200	2.2	1×10^{-13}

constrains larger grains.

From an atomic perspective, the grain growth is a diffusion process in which atoms diffuse across the grain boundary by thermal activation. The thermal-activation nature of the grain-growth law described in Eq. (1) is embedded in the constant, k, which is an Arrhenius-type equation written as [42].

$$k = k_0 \exp\left(-\frac{Q_g}{RT}\right) \tag{12}$$

where k_0 is a constant taking into account the activation energy of grain boundaries, Q_g is the activation energy, T is the temperature, and R is the gas constant. Taking the logarithm to both sides of Eq. (12) reaches

$$\ln k - \ln k_0 = \left(-\frac{Q_g}{RT}\right) \tag{13}$$

with which we can perform a linear fit to the $\ln k$ against $1/T$ data to obtain the activation energy, Q_g, from the slope. As demonstrated in Fig. 5, Q_g is determined to be 303 kJ/mol for the HfNbTaZrTi RHEA in study. However, the linearity is not good. The three data points are thought to give two slopes between 1,000 and 1,100 °C, and between 1,100 and 1,200 °C, respectively since two different mechanisms might be involved. Under this condition, two activation energies are obtained, that is, 205 kJ/mol between 1,000 and 1,100 °C, and 401 kJ/mol between 1,100 and 1,200 °C. As compared with that activation energy, 389 kJ/mol, obtained from grain-growth experiment at 1,200, 1,250, 1,300 and 1,350 °C after cold rolling by the 70% reduction in thickness for the same alloy [35] and that the activation energy of 246 kJ/mol obtained at 1,100 °C in a homogenized, cold-forged, and then 89% cold-rolled HfNbTaZrTi RHEA [36], it indicates that the activation energy is higher in the higher annealing temperature range and lower in the lower temperature range.

3.3. Effect of grain size on mechanical properties

Annealing the RHEA samples at 1,000, 1,100, and 1,200 °C for 6 h produces an average grain sizes of 40, 87, and 112 μm, respectively. The engineering stress – strain curves of these coarse- and fine-grained specimens measured from uniaxial tension are provided in Fig. 6, from which it is evident that the flow stress of the HEAs increases as the grain size decreases. Some key material properties, such as the yield strength taken at a plastic strain of 0.2%, ultimate tensile strength (UTS), and elongation, are extracted from the curves and listed in Table 3. The HEA with the smallest grain size of 40 μm exhibits the highest yield strength of 985 MPa, followed by 972 MPa for the specimen with a grain size of 87 μm, and then 967 MPa for the specimen with a grain size of 112 μm. The same trend holds for the ultimate tensile strength (UTS) as well, as indicated in Fig. 6 and Table 3. It is noted that the work hardening of the present RHEA during tension is quite low, which results in small increase in strength up to UTS. The reason for this trend is attributable to its distorted whole-solute BCC matrix with the high-strength and large lattice distortion, which could potentially raise the driving force to reduce the overall strain energy and induce the dynamic recovery [35]. Actually, the calculated lattice distortion in our treated HEAs is much higher than the reported ones [43].

The effectiveness of the grain refinement in enhancing the strength of polycrystalline metals is known to be ascribed to the grain-boundary hardening, and can be quantified by the well-known Hall-Petch relation [44–46].

$$\sigma_y = \sigma_0 + k_{HP} D^{-0.5} \tag{14}$$

where σ_y is the yield strength, D is the average grain size, σ_0 is a constant that can be considered as either the frictional stress induced by dislocation motions or internal back stresses [46], k_{HP} is a constant that can be viewed as a measure of the grain-boundary resistance to slip transfer [46].

We apply this classical equation to our RHEA by plotting the experimental yield strength as a function of $D^{-0.5}$ in Fig. 7 and fitting the data with Eq. (14). From the fitting curve, σ_0 and k_{HP} can

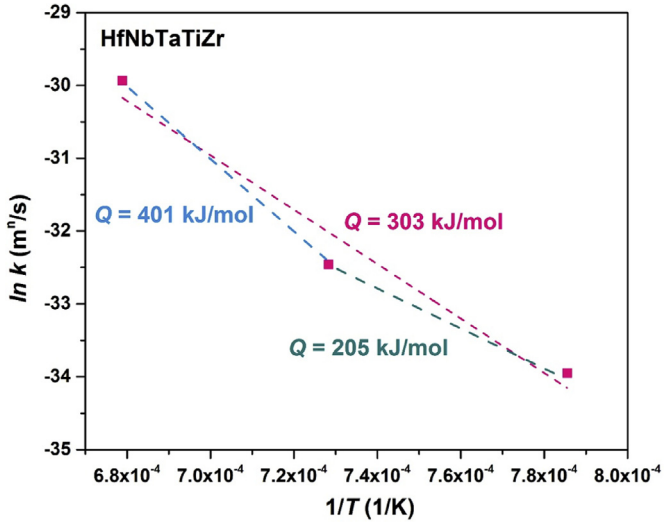

Fig. 5. Linear fitting of Eq. (13) to *lnk*data against $1/T$, from which the activation energies, Q_g, are obtained from the slopes.

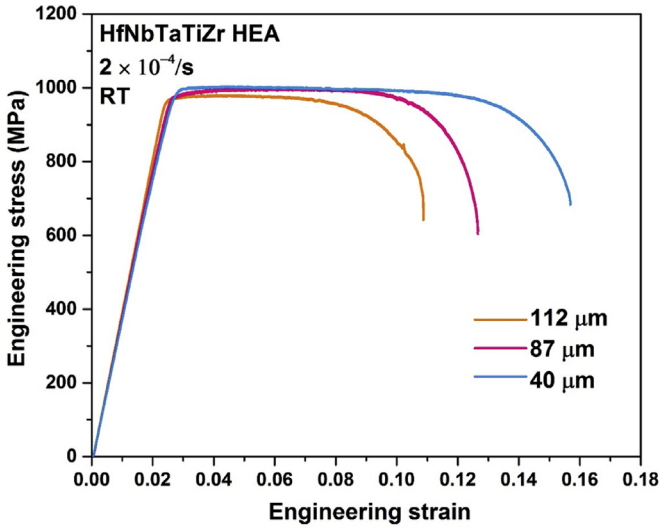

Fig. 6. Uniaxial tensile true stress – strain curves of the HfNbTaTiZr HEAs with the grain sizes of 40, 87, and 112 μm, tested at room temperature and a strain rate of 2×10^{-4} s^{-1}.

Table 3
The dependence of yield strength, UTS, and elongation on grain sizes.

Grain size (μm)	Yield strength (MPa)	UTS (MPa)	Fracture elongation (in strain)
40	985	1,004	0.157
87	972	999.5	0.126
112	967	980.6	0.108

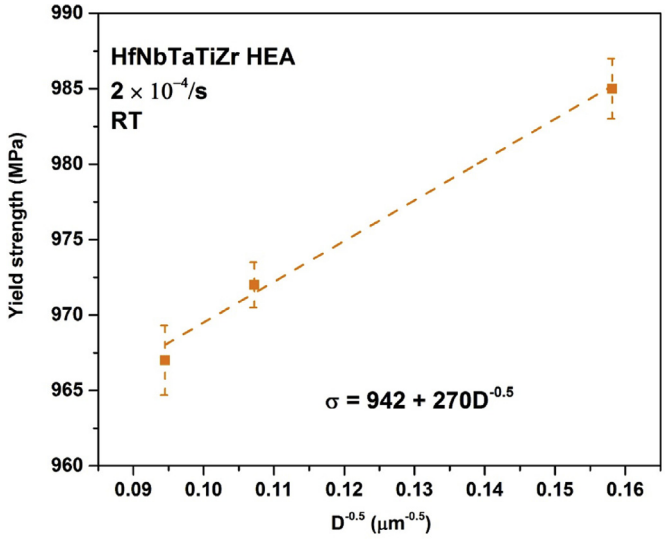

Fig. 7. Linear fitting of Hall-Petch relation [i.e., Equation (14)] to the experimental yield strength data as a function of $D^{-0.5}$ for the HfNbTaTiZr HEAs, from which σ_0 and k_{HP} are determined to be 942 MPa and 270 MPa/μm$^{-1/2}$ from the intercept and slope, respectively.

be retrieved as 942 MPa and 270 MPa/μm$^{-1/2}$ from the intercept and slope, respectively. Ultimately, the Hall-Petch relation for the present HfNbTaZrTi HEA has the form of $\sigma_y = 942 + 270D^{-0.5}$. For a better comparison of the friction stress σ_0 and k_{HP} in various alloys, the data for other alloys is retrieved from the literatures [33–55] and plotted in Fig. 8 along with ours. It is apparent that the RHEA in the present work exhibits a much higher friction stress than that of the AISI 301 stainless steel, Mo, Nb and W alloys [47], and CoCrFeMnNi HEAs, etc. However, the k_{HP} value in the current HfNbTaTiZr RHEA is found to be much lower than that in the 316 stainless steel, CoCrFeMnNi, and $Al_{0.3}$CoCrFeNi HEAs. This trend is interesting and reasonable by the consideration of the low work hardening in the present RHEA. In fact, grain size strengthening is preferentially explained by the pre-working hardening along grain boundaries before macroyielding, which has been verified by TEM observation of deformation zone along grain boundaries [48].

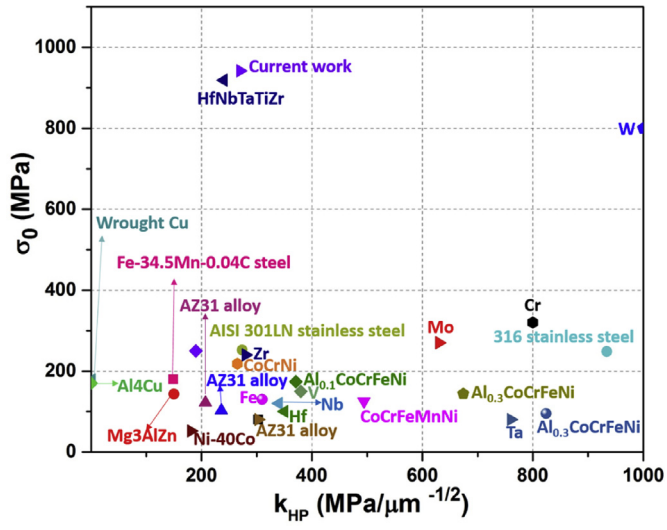

Fig. 8. The comparison of σ_0 and k_{HP} between the current HEA and conventional alloys [33–55].

Before macro-yielding, the preferential yielding and plastic deformation along grain boundaries induced by the elastic incompatibility among neighboring grains in the elastic region explains the grain-size-strengthening effect [48]. Thus, the low work hardening in the present RHEA, as seen in the Fig. 6, would give a low k_{HP} value of the grain boundary strengthening. This feature also informs us that high working hardening alloys such as the 316 stainless steel, CoCrFeMnNi, and $Al_{0.3}$CoCrFeNi HEAs would have high k_{HP}.

4. Discussion

A typical value of $n = 2$ is usually noted for pure metals, in which diffusion governs the grain-growth kinetics. n values larger than 2, however, are often found in solid-solution alloys because of solute dragging effects at grain boundaries. In light of this assertion, Juan et al. [35] found a large value of $n = 3.5$ in the cold-rolled and annealed HfNbTaZrTi RHEA. They proposed that the solute-drag effect is significant in the whole-solute matrix of HEAs, as compared with the conventional solid-solution alloy. This trend is related to the energy incurred during different sizes of abundant solutes along grain boundaries in-situ adjusting their relative positions to form the low-energy configuration of grain boundaries during boundary migration. In the cold-rolled and annealed HfNbTaZrTi RHEA studied in the present work, $n = 2.2–2.4$ is slightly larger than the typical value of 2 for pure metals, suggesting that chemical segregation and solute drag also play a major role in slowing down grain growth [41]. It is noted that the main difference in the processing is the annealing temperature range: Juan's work used the annealing temperature from 1,200 to 1,350 °C whereas the present work was conducted from 1,000 to 1,200 °C. As the degree of short-range chemical order due to the bonding difference among atomic pairs is higher in the lower temperature range and lower in the higher one, it suggests that retardation to grain boundary migration is smaller with a lower degree of short range ordering at higher temperatures. This trend means that a more random distribution of solute atoms yields a larger drag force to grain boundary. The phenomenon can be explained because the tendency to obtain the low-energy configuration of grain boundaries during boundary migration by in-situ adjustment of the abundant solutes along grain boundaries would be more significant than that with abundant short range order clusters which are already in the lower energy state [56–60]. This explanation is related to the abundant solutes in the random solid-solution state, a mechanism not found in conventional alloys based on one major element and a low concentration of solute atoms. This feature means that the phenomenon and its mechanism are new for the HEA system. As grain boundaries are high diffusion paths, the in-situ pinning along these paths continues even as they migrate. On the other hand, short-range ordering gives a cluster distribution, preferentially Nb, Ta-rich, and Hf, Ti, Zr-rich clusters due to their chemical compatibility, as discussed by Senkov et al. [36]. These clusters disperse in grain interiors to consume most solute atoms in the remaining matrix and reduce the in-situ pinning force on grain boundaries. As clusters of short range are nano-sized, they do not behave like large precipitates or inclusions to give Zener pinning. Therefore, they have a limited contribution to the drag force as grain boundaries sweep across them.

On the other hand, Senkov's work gave $n = 2$ or 3 for the temperature of 1,100 °C, indicating a lower drag force to the grain-boundary migration [36]. This feature could be explained with the fact that Senkov's sample received a homogenization treatment at 1,200 °C for 24 h, by which dendrite and interdendrite segregations were mostly eliminated to give a more random distribution of

solutes, compared with that of the present work. This feature means that the preferential Nb, Ta-rich, and Hf, Ti, Zr-rich clusters of greater amounts would form in the homogeneous matrix [36] in comparison with the present alloy without a homogenization treatment.

Since the grain growth is a diffusion process in nature, the activation energy also plays a crucial role. Equation (10) essentially links the activation energy with the constant, *k*, in the governing equation of grain growth. In the present study, the activation energy for the HfNbTaTiZr RHEA is determined as $Q_g = 303$ kJ/mol. However, as pointed out in Section 3.2, the activation-energy value is from an average of two slopes between 1,000 and 1,100 °C, and between 1,100 and 1,200 °C. Two activation energies are obtained: 205 kJ/mol between 1,000 and 1,100 °C, and 401 kJ/mol between 1,100 and 1,200 °C. Compared with the activation energy, 389 kJ/mol, obtained from 1,200 to 1,350 °C in the same alloy and same preparation process by Juan et al. [35], and that of 238 kJ/mol, obtained from 1,100 to 1,200 °C in the same alloy but with a pre-homogenization treatment by Senkov et al. [36], the present two-stage activation energies demonstrate that two mechanisms are likely to be involved in the two temperature ranges. As stated above, the higher activation energy from 1,200 to 1,350 °C relates with a higher degree of disorder, i.e., a more random state. The mechanism explaining for n = 3.5 and high activation energy of 389 kJ/mol is directly associated with the volume diffusion through the lattice, whose rate is controlled by the slowest species, i.e. Nb and Ta. The slow species are the controlling factors during the diffusion process. The migration of grain boundaries cannot proceed without increasing the energy except that the average composition is maintained, which could be controlled by the slow ones that determine the reaction rate. On the other hand, the smaller activation energy from 1,000 to 1,100 °C is related to a higher degree of short range order, preferentially Nb, Ta-rich, and Hf, Ti, Zr-rich clusters due to their chemical compatibility [56–60]. The cluster distribution in the matrix would have less problem in waiting for the slow ones in keeping the homogenous equiatomic composition. As a result, the activation energy is no longer determined by Nb and Ta and thus has a lower value.

5. Conclusion

The grain growth of the cast HfNbTaTiZr HEA, subsequent to cold-rolling and annealing at 1,000–1,200 °C for up to 24 h, was investigated. Experimental results determine the grain-growth exponent and average activation energy to be $n = 2.2–2.4$ and $Q_g = 303$ kJ/mol, respectively. Two activation energies can also be obtained: 205 kJ/mol between 1,000 and 1,100 °C, and 401 kJ/mol between 1,100 and 1,200 °C. This trend indicates that two mechanisms are involved and the transition temperature is around 1,100 °C. The higher activation energy relates with a greater degree of disorder, i.e., a more random state. Grain boundary migration needs the volume diffusion through the chemically-homogeneous lattice, whose rate is controlled by the slowest species, Nb and Ta. The grain-size strengthening follows the Hall-Petch relation in the form of $\sigma_y = 942 + 270D^{-0.5}$. The low k_{HP} coefficient, 270 MPa/μm$^{-1/2}$, is consistent with the low work hardening of the present RHEA since work hardening along grain boundaries could enhance the macro-yield strength.

Acknowledgements

We are grateful for the support of the Department of Energy (DOE) Office of Fossil Energy, National Energy Technology Laboratory (NETL) (DE-FE-0011194) and the National Science Foundation (DMR-1611180 and 1809640), with Drs. J. Mullen, V. Cedro, R. Dunst, S. Markovich, G. Shiflet, and D. Farkas as program managers. P.K. Liaw very much appreciate the support from the U.S. Army Office Project (W911NF-13-1-0438 and W911NF-19-2-0049) with the program managers, Drs. M. P. Bakas, S. N. Mathaudhu, and D. M. Stepp. S.Y. Chen and P.K. Liaw would like to acknowledge the financial support of the Center for Materials Processing (CMP), at The University of Tennessee, with the Director of Dr. Claudia J. Rawn. The current research used resources of the National Energy Research Scientific Computing Center (NERSC), a U.S. Department of Energy Office of Science User Facility operated under Contract No. of DE-AC02-05CH11231. J.W. Yeh would like to thank the financial support by the "High Entropy Materials Center" from The Featured Areas Research Center Program within the framework of the Higher Education Sprout Project by the Ministry of Education (MOE) and from the Project of MOST 107-3017-F-007-003 by the Ministry of Science and Technology (MOST) in Taiwan. XRD was performed at the Joint Institute for Advanced Materials (JIAM) Diffraction Facility, located at the University of Tennessee, Knoxville.

References

[1] J.W. Yeh, S.K. Chen, S.J. Lin, J.Y. Gan, T.S. Chin, T.T. Shun, C.H. Tsau, S.Y. Chang, Nanostructured high-entropy alloys with multiple principal elements: novel alloy design concepts and outcomes, Adv. Eng. Mater. 6 (5) (2004) 299–303.
[2] B. Cantor, I.T.H. Chang, P. Knight, A.J.B. Vincent, Microstructural development in equiatomic multicomponent alloys, Mater. Sci. Eng. A 375–377 (2004) 213–218.
[3] O.N. Senkov, G.B. Wilks, D.B. Miracle, C.P. Chuang, P.K. Liaw, Refractory high-entropy, Intermetallics 18 (2010) 1758–1765.
[4] O.N. Senkov, J.M. Scott, S.V. Senkova, D.B. Miracle, C.F. Woodward, Microstructure and room temperature properties of a high-entropy TaNbHfZrTi alloy, J. Alloys Compd. 509 (2011) 6043–6048.
[5] S.Y. Chen, Y. Tong, K.-K. Tseng, J.W. Yeh, D. Poplawsky, J.G. Wen, M.C. Gao, G. Kim, W. Chen, Y. Ren, R. Feng, W.D. Li, P.K. Liaw, Phase transformations of HfNbTaTiZr high-entropy alloy at intermediate temperatures, Scripta Mater. 158 (2019) 50–56.
[6] S.Y. Chen, X. Xie, B.L. Chen, J.W. Qiao, Y. Zhang, Y. Ren, K.A. Dahmen, P.K. Liaw, Effects of temperature on serrated flows of $Al_{0.5}$CoCrCuFeNi high-entropy alloy, JOM 67 (10) (2015) 2314–2320.
[7] Y. Zhang, T.T. Zuo, Z. Tang, M.C. Gao, K.A. Dahmen, P.K. Liaw, Z.P. Lu, Microstructures and properties of high-entropy, Prog. Mater. Sci. 61 (2014) 1–93.
[8] S. Chen, X. Xie, W. Li, R. Feng, B. Chen, J. Qiao, Y. Ren, Y. Zhang, K.A. Dahmen, P.K. Liaw, Temperature effects on the serrated behavior of an Al 0.5 CoCrCuFeNi high-entropy alloy, Mater. Chem. Phys. 210 (2018) 20–28.
[9] J. Brechtl, S.Y. Chen, X. Xie, Y. Ren, J.W. Qiao, P.K. Liaw, S.J. Zinkle, Towards a greater understanding of serrated flows in an Al-containing high entropy-based, Int. J. Plast. 115 (2019) 71–92.
[10] M. Feuerbacher, M. Heidelmann, C. Thomas, Hexagonal high-entropy alloys, Mater. Res. Lett. 3 (1) (2014) 1–6.
[11] L. Lilensten, J.P. Couzinié, L. Perrière, J. Bourgon, N. Emery, I. Guillot, TaNbHfZrTi New structure in refractory high-entropy alloys, Mater. Lett. 132 (2014) 123–125.
[12] K.M. Youssef, A.J. Zaddach, C. Niu, D.L. Irving, C.C. Koch, A novel low-density, high-hardness, high-entropy alloy with close-packed single-phase nanocrystalline structures, Mater. Res. Lett. 3 (2) (2014) 95–99.
[13] M.C. Gao, B. Zhang, S.M. Guo, J.W. Qiao, J.A. Hawk, High-entropy alloys in hexagonal close-packed structure, Metall. Mater. Trans. 47 (7) (2015) 3322–3332.
[14] D.B. Miracle, O.N. Senkov, A critical review of high entropy alloys and related concepts, Acta Mater. 122 (2017) 448–511.
[15] O.N. Senkov, J.M. Scott, F. Meisenkothen, S.V. Senkova, D.B. Miracle, C.F. Woodward, Microstructure and elevated temperature properties of a refractory TaNbHfZrTi alloy, J. Mater. Sci. 47 (2012) 4062–4074.
[16] O.N. Senkov, G.B. Wilks, J.M. Scott, D.B. Miracle, Mechanical properties of $Nb_{25}Mo_{25}Ta_{25}W_{25}$ and $V_{20}Nb_{20}Mo_{20}Ta_{20}W_{20}$ refractory high entropy alloys, Intermetallics 19 (2012) 698–706.
[17] M.H. Chuang, M.H. Tsai, W.R. Wang, S.J. Lin, J.W. Yeh, Microstructure and wear behavior of $Al_xCo_{1.5}CrFeNi_{1.5}Ti_y$ high-entropy alloys, Acta Mater. 59 (2011) 6308–6317.
[18] Y. Shi, B. Yang, X. Xie, J. Brechtl, K.A. Dahmen, P.K. Liaw, Corrosion of Al_x-CoCrFeNi high-entropy alloys: Al-content and potential scan-rate dependent pitting behavior, Corros. Sci. 119 (2017) 33–45.
[19] Y. Shi, B. Yang, P.K. Liaw, Corrosion-resistant high-entropy alloys: a review, Metals 7 (2) (2017) 1–18.
[20] W.D. Li, G. Wang, S.W. Wu, P.K. Liaw, Creep, fatigue, and fracture behavior of high-entropy alloys, J. Mater. Res. 33 (19) (2018) 3011–3034.

[21] S.Y. Chen, W.D. Li, X. Xie, J. Brechtl, B.L. Chen, P.Z. Li, G.F. Zhao, F.Q. Yang, J.W. Qiao, K.A. Dahmen, P.K. Liaw, Nanoscale serration and creep characteristics of $Al_{0.5}$CoCrCuFeNi high-entropy alloys, J. Alloys Compd. 752 (2018) 464–475.
[22] W.D. Li, P.K. Liaw, Y.F. Gao, Fracture resistance of high entropy alloys: a review, Intermetallics 99 (2018) 69–83.
[23] B. Guennec, V. Kentheswaran, L. Perrière, A. Ueno, I. Guillot, J-Ph. Couzinié, G. Dirras, Four-point bending fatigue behavior of an equimolar BCC HfNbTaTiZr high-entropy alloy: macroscopic and microscopic viewpoints, Materialia 4 (2018) 348–360.
[24] M.A. Hemphill, T. Yuan, G.Y. Wang, J.W. Yeh, C.W. Tsai, A. Chuang, P.K. Liaw, Fatigue behavior of $Al_{0.5}$CoCrCuFeNi high entropy alloys, Acta Mater. 60 (16) (2012) 5723–5734.
[25] Z. Tang, T. Yuan, C.W. Tsai, J.W. Yeh, C.D. Lundin, P.K. Liaw, Fatigue behavior of a wrought $Al_{0.5}$CoCrCuFeNi two-phase high-entropy alloy, Acta Mater. 99 (2015) 247–258.
[26] S. Shukla, T. Wang, S. Cotton, R.S. Mishra, Hierarchical microstructure for improved fatigue properties in a eutectic high entropy alloy, Scripta Mater. 156 (2018) 105–109.
[27] K. Liu, M. Komarasamy, B. Gwalani, S. Shukla, R.S. Mishra, Fatigue behavior of ultrafine grained triplex $Al_{0.3}$CoCrFeNi high entropy alloy, Scripta Mater. 158 (2019) 116–120.
[28] K.V.S. Thurston, B. Gludovatz, A. Hohenwarter, G. Laplanche, E.P. George, R.O. Ritchie, Effect of temperature on the fatigue-crack growth behavior of the high-entropy alloy CrMnFeCoNi, Intermetallics 88 (2017) 65–72.
[29] P. Chen, C. Lee, S.Y. Wang, M. Seifi, J.J. Lewandowski, K.A. Dahmen, H. Jia, X. Xie, B. Chen, J.W. Yeh, C.W. Tsai, T. Yuan, P.K. Liaw, Fatigue behavior of high-entropy alloys: a review, Sci. China Technol. Sci. 61 (2) (2017) 168–178.
[30] B. Gludovatz, A. Hohenwarter, D. Catoor, E.H. Chang, E.P. George, R.O. Ritchie, A fracture-resistant high-entropy alloy for cryogenic applications, Science 345 (6201) (2014) 1153–1160.
[31] W.H. Liu, Y. Wu, J.Y. He, T.G. Nieh, Z.P. Lu, Grain growth and the Hall–Petch relationship in a high-entropy FeCrNiCoMn alloy, Scripta Mater. 68 (7) (2013) 526–529.
[32] Z. Wu, H. Bei, F. Otto, G.M. Pharr, E.P. George, Recovery, recrystallization, grain growth and phase stability of a family of FCC-structured multi-component equiatomic solid solution alloys, Intermetallics 46 (2014) 131–140.
[33] G. Dan Sathiaraj, P.P. Bhattacharjee, Effect of cold-rolling strain on the evolution of annealing texture of equiatomic CoCrFeMnNi high entropy alloy, Mater. Char. 109 (2015) 189–197.
[34] O.N. Senkov, S.L. Semiatin, Microstructure and properties of a refractory high-entropy alloy after cold working, J. Alloys Compd. 649 (2015) 1110–1123.
[35] C.-C. Juan, M.-H. Tsai, C.W. Tsai, W.L. Hsu, C.M. Lin, S.-K. Chen, S.J. Lin, J.W. Yeh, Simultaneously increasing the strength and ductility of a refractory high-entropy alloy via grain refining, Mater. Lett. 184 (2016) 200–203.
[36] O.N. Senkov, A.L. Pilchak, S.L. Semiatin, Effect of cold deformation and annealing on the microstructure and tensile properties of a HfNbTaTiZr refractory high entropy alloy, Metall. Mater. Trans. 49 (7) (2018) 2876–2892.
[37] C.M. Cepeda-Jiménez, J.M. Molina-Aldareguia, M.T. Pérez-Prado, Effect of grain size on slip activity in pure magnesium polycrystals, Acta Mater. 84 (2015) 443–456.
[38] J.E. Burke, D. Turnbull, Recrystallization and grain growth, Prog. Met. Phys. 3 (1952) 220–292.
[39] H.V. Atkinson, Overview no. 65 Theories of normal grain growth in pure single phase systems, Acta Metall. 36 (3) (1988) 469–491.
[40] B. Cherukuri, R. Srinivasan, S. Tamirisakandala, D. Miracle, The influence of trace boron addition on grain growth kinetics of the beta phase in the beta titanium alloy Ti–15Mo–2.6Nb–3Al–0.2Si, Scripta Mater. 60 (7) (2009) 496–499.
[41] Y.F. Xu, D.Q. Yi, H.Q. Liu, B. Wang, F.L. Yang, Age-hardening behavior, microstructural evolution and grain growth kinetics of isothermal ω phase of Ti–Nb–Ta–Zr–Fe alloy for biomedical applications, Mater. Sci. Eng. A 529 (2011) 326–334.
[42] T. Wang, H. Guo, L. Tan, Z. Yao, Y. Zhao, P. Liu, Beta grain growth behaviour of TG6 and Ti17 titanium alloys, Mater. Sci. Eng. A 528 (21) (2011) 6375–6380.
[43] C. Lee, G. Song, M.C. Gao, R. Feng, P. Chen, J. Brechtl, Y. Chen, K. An, W. Guo, J.D. Poplawsky, S. Li, A.T. Samaei, W. Chen, A. Hu, H. Choo, P.K. Liaw, Lattice distortion in a strong and ductile refractory high-entropy alloy, Acta Mater. 160 (2018) 158–172.
[44] E.O. Hall, The deformation and ageing of mild steel: III discussion of results, Proc. Phys. Soc. B64 (1951) 747–753.
[45] N.J. Petch, The cleavage strength of polycrystals, J. Iron Steel Inst. 174 (1953) 25–28.
[46] N. Hansen, Hall–Petch relation and boundary strengthening, Scripta Mater. 51 (2004) 801–806.
[47] Z.C. Cordero, B.E. Knight, C.A. Schuh, Six decades of the Hall Petch effect a survey of grain size strengthening studies on pure metals, Int. Mater. Rev. 61 (2016) 495–512.
[48] M.A. Meyers, K.K. Chawla, Mechanical Metallurgy-Principles and Applications, Prentice-Hall, Inc., New Jersey, 1984, pp. 502–506.
[49] X.H. Dong, X.T. Hong, F. Chen, B.R. Sang, W. Yu, X.P. Zhang, Effects of specimen and grain sizes on compression strength of annealed wrought copper alloy at room temperature, Mater. Des. 64 (2014) 400–406.
[50] L.L. Chang, Y.N. Wang, X. Zhao, M. Qi, Grain size and texture effect on compression behavior of hot-extruded Mg–3Al–1Zn alloys at room temperature, Mater. Char. 60 (9) (2009) 991–994.
[51] J.A. del Valle, F. Carreño, O.A. Ruano, Influence of texture and grain size on work hardening and ductility in magnesium-based alloys processed by ECAP and rolling, Acta Mater. 54 (16) (2006) 4247–4259.
[52] H.Y. Yasuda, H. Miyamoto, K. Cho, T. Nagase, Formation of ultrafine-grained microstructure in Al 0.3 CoCrFeNi high entropy alloys with grain boundary precipitates, Mater. Lett. 199 (2017) 120–123.
[53] S. Yoshida, T. Bhattacharjee, Y. Bai, N. Tsuji, Friction stress and Hall-Petch relationship in CoCrNi equi-atomic medium entropy alloy processed by severe plastic deformation and subsequent annealing, Scripta Mater. 134 (2017) 33–36.
[54] B. Kang, J. Lee, H.J. Ryu, S.H. Hong, Ultra-high strength WNbMoTaV high-entropy alloys with fine grain structure fabricated by powder metallurgical process, Mater. Sci. Eng. A 712 (2018) 616–624.
[55] B. Kang, J. Lee, H.J. Ryu, S.H. Hong, Microstructure, mechanical property and Hall-Petch relationship of a light-weight refractory Al 0.1 CrNbVMo high entropy alloy fabricated by powder metallurgical process, J. Alloys Compd. 767 (2018) 1012–1021.
[56] F. Otto, A. Dlouhý, C. Somsen, H. Bei, G. Eggeler, E.P. George, The influences of temperature and microstructure on the tensile properties of a CoCrFeMnNi high-entropy alloy, Acta Mater. 61 (15) (2013) 5743–5755.
[57] S. Maiti, W. Steurer, Structural-disorder and its effect on mechanical properties in single-phase TaNbHfZr high-entropy alloy, Acta Mater. 106 (2016) 87–97.
[58] M. Gao, D. Alman, Searching for next single-phase high-entropy alloy compositions, Entropy 15 (10) (2013) 4504–4519.
[59] O.N. Senkov, D.B. Miracle, K.J. Chaput, J.-P. Couzinie, Development and exploration of refractory high entropy alloys—a review, J. Mater. Res. (2018) 1–37.
[60] S.I. Rao, C. Varvenne, C. Woodward, T.A. Parthasarathy, D. Miracle, O.N. Senkov, W.A. Curtin, Atomistic simulations of dislocations in a model BCC multicomponent concentrated solid solution alloy, Acta Mater. 125 (2017) 311–320.